# Reverse Engineering at the Atomic Scale: Competitive Analysis of a Gallium-Nitride-Based Commercial Light-Emitting Diode

**A.D. Giddings*, T.J. Prosa, D. Olson, P.H. Clifton, and D.J. Larson**
CAMECA Instruments, Inc., 5500 Nobel Dr., Madison, WI 53711
*giddings@physics.org



## Introduction

The consumer electronics market is forecast to be valued at 1.6 trillion US Dollars by 2018 [1]. The massive investment required to maintain leadership in this highly competitive market is protected by a bevy of intellectual property disclosures and trade secrets; a single semiconductor product may be covered by more than ten-thousand patents [2]. An example of the bitter litigation that can ensue when semiconductor companies lock horns over intellectual property is the protracted, continent-spanning broadside of lawsuits between Nichia Corporation and Seoul Semiconductor Company. This conflict over light-emitting diode (LED) technologies started in 2006 and eventually culminated in 2009 with cross-licensing agreements between the two companies [3–4].

The nanometer scale and the embedded nature of semiconductor devices, such as LEDs, means that there has been little recourse for physically confirming suspected infringement. However, advancements in microscopy techniques over the past decade now enable unprecedented levels of detail in characterization, as well as new types of analysis. One of the principle tools that has enabled this revolution in nano-analysis is the atom probe microscope [5]; this instrument is able to determine the 3D structure and composition of a material, at near-atomic scales. The possible ramifications of these new capabilities on reverse engineering or "competitive analysis" are exhibited in this article with an atom probe characterization of the light-producing region of a GaN-based LED, similar to the kinds of devices that had been under litigation [6].

## GaN-Based Quantum Well Light Emitting Diodes

**Light-Emitting Diodes.** LEDs are light sources based on the recombination of carriers in doped semiconductor materials. In its most basic form an LED consists of a p-doped region and an n-doped region that together form a diode where electrons and holes recombine under the influence of an external voltage, producing photons. Although a wide variety of semiconductor materials can be used to make LEDs, most modern devices are based on the compound semiconductor GaN. This material has proved successful because it possesses a number of critical technical properties, particularly the ability to provide a range of colors with a high-output brightness.

**Adding a third element.** The key to GaN's utility lies in the fact that by alloying the GaN with a third element, typically aluminum or indium, the electronic band structure of the material can be modified [7–8]. Furthermore, epitaxial growth allows precise control over the layer structure and composition. The peak electroluminescence emission wavelength depends on the band structure, so the color of the LED can be engineered by choosing the appropriate composition. As a result, LEDs that are based on GaN are capable of wide color gamut, covering nearly the entire range of the visible spectrum, as well as near-infrared and ultraviolet wavelengths.

High breakdown voltages and charge carrier saturation velocities make GaN very suitable for high-power applications. To get good output brightness, an LED needs to possess high quantum efficiency, that is, a large fraction of the carrier recombinations produce a photon. Having a simple homogeneous structure is not very efficient because the carriers injected across the diode travel varying distances, making the active area diffuse and requiring a high current density.

**Multilayer structures.** This situation is improved by using a heterogeneous structure, that is, a multilayer of materials with different compositions. Taking advantage of the fact that the band structures can be engineered through composition control, carriers can be confined within a layer by sandwiching a narrower bandgap material between two wider bandgap materials. When this is used for the active region of an LED device, the efficiency of carrier recombination is improved. Such structures are known as double heterostructures, or when the dimensions are reduced to the point that quantum confinement effects occur, quantum wells (QWs) are formed. Not only do QWs offer greater efficiency, further improvements can be obtained when a series of QWs are chained together to form a multiple quantum well (MQW).

Similar to the MQW, a superlattice (SL) is another nanostructural feature that can be engineered into the epitaxially grown semiconductor materials. An SL is a periodic arrangement of two materials with layer thicknesses of less than 10 nm. With MQWs each QW is isolated from the next, whereas with an SL the barriers are thinner, so each QW is coupled, resulting in special optical or electronic properties. An SL may be used in an LED device as the active, light-producing region, but it also may be included as a low-resistance layer to carry charge [9], as a barrier to control formation of efficiency-reducing crystal defects such as dislocations and pin-holes [10–11], or as a distributed Bragg reflector to control the direction of photon propagation [12].

Another kind of feature that can be included in an LED device is an electron-blocking layer (EBL). This is a region of wider bandgap situated between the p-doped layer and the active region. Electrons have a higher diffusivity than holes, so the electron-blocking layer prevents them from entering the p-doped region, ensuring that the recombination occurs in the active region.

**3D nanostructures.** All the features described so far have been planar in form; however, even more complex and subtle structures could potentially appear in GaN LEDs. For example, devices have been designed with 3D inclusions in the MQW, with dimensions on the order of 10 nm. These inclusions are designed to both improve efficiency and reduce dislocations that occur when growing the LED layers on lower-cost, non-lattice matched substrates such as Si [13]. In fact, a patent for such a structure was one of the subjects of the litigation between the Nichia and the Seoul Semiconductor [14].

As such, these quantum-electronic devices are highly engineered in order to achieve specific operational criteria. Not only is the resultant light color important, but factors such as maximum brightness, luminous efficacy, power characteristics, durability, production yield, and cost will determine whether a product is successful in the marketplace. Each of these properties will be directly influenced by the nano-structural composition of the device. Examining a rival product in order to understand the technology and processes used in the design, manufacture, or operation may be critical for remaining competitive. However, the complex structural and compositional nature of these devices necessitates the use of an analysis method capable of achieving suitable 3D spatial resolution and chemical sensitivity.

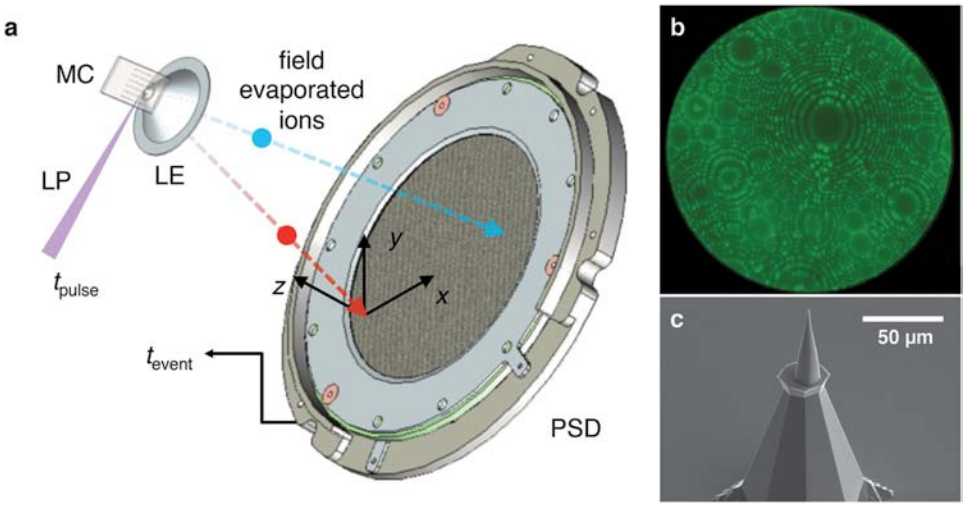


**Figure 1:** (a) Schematic showing the principles of a LEAP. Labeled in the diagram are the Si microtip coupon (MC), the local electrode (LE), the laser pulse (LP), and the position sensitive detector (PSD); $t_{pulse}$ is the time that the laser pulse triggers field evaporation of ions from the specimen on the coupon, and $t_{event}$ is the time the ion reaches the detector. (b) An example of a typical FIM image obtained from a W specimen using He imaging gas at a pressure of $9\times10^{-5}$ Pa. (c) SEM image of a single microtip for FIB lift-out mounting.

## Atom Probe Tomography

An atom probe tomography (APT) dataset is comprised of a list of ions whose chemical species and spatial coordinates are individually specified. This dataset is processed and visualized to create a graphical representation from which pertinent information can be extracted. To appreciate how such unique data can be obtained, it is necessary to understand the basic principles underpinning APT, a technique made possible through the marriage of the field ion microscope (FIM) and the time-of-flight (TOF) mass-spectrometer [15]. Figure 1a shows the operating principles of a commercial instrument, the local electrode atom probe (LEAP).

An FIM is a point projection microscope that can obtain surface magnifications greater than a million times. When a high voltage is applied to a needle-shaped specimen in the presence of a rarified gas atmosphere, gas atoms are polarized by the strong electric field and are attracted to the tip apex. As the atoms settle onto the surface, there is a probability that they will become ionized and will be repelled outward from the specimen. An ion current is produced in relation to the field strength localized to the tip surface; the points of highest curvature, such as atoms at low coordination (step edges) sites, ionize the imaging gas most frequently. When a phosphor screen is placed to intercept the ion current, a projected image of the positions of these edge atoms is created. Figure 1b shows an example of an FIM image where the atomic surface crystallography is clearly visible.

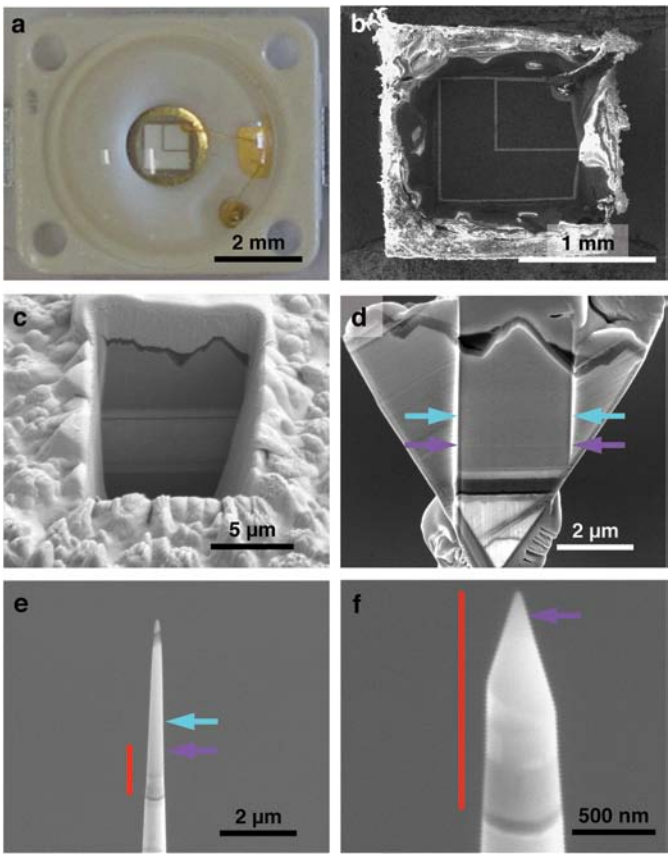


**Figure 2:** The LED device through various stages of deprocessing and APT specimen preparation. (a) Light microscopy photo of the purchased device. (b) through (f) are a sequence of SEM images (b) after depackaging by polishing to expose the wafer, (c) after cutting into the surface by FIB, (d) after a lamella has been lifted out of the surface, inverted, and mounted onto a microtip coupon, (e) after annular FIB milling has formed a tip shape, and (f) after a final low-energy FIB mill has taken down the tip to the region of interest. The cyan and indigo arrows in (d–f) highlight two regions of different contrast revealed by a face peel into the end of lamella. The vertical red lines in (e) and (f) indicate the same volume before and after the final mill.

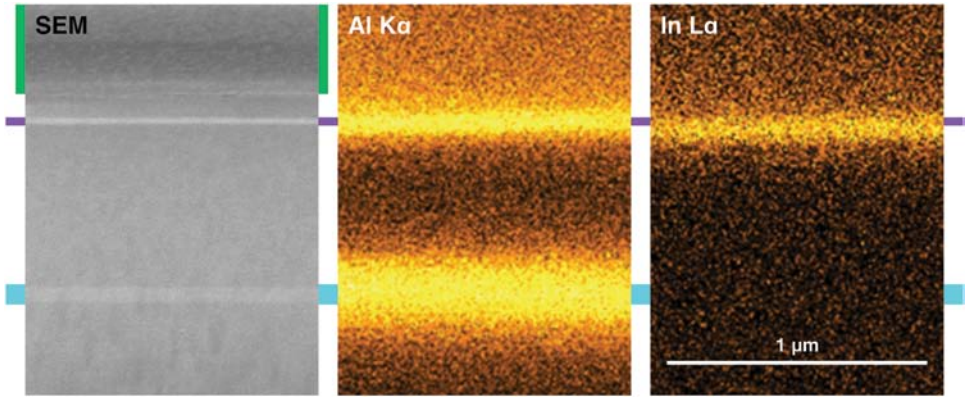


**Figure 3:** SEM image of a cross section of the device (left) with the corresponding EPMA compositional maps (center and right). In the SEM image two regions of lighter contrast are highlighted by indigo and cyan boarders. The green border is an IBID-Pt processing cap. Note that the sample mounting is inverted from Figure 2d. The central image, showing the Al Kα X-ray map, reveals that these two volumes contain Al. The right image, the In Lα map, shows that the upper layer also contains In.

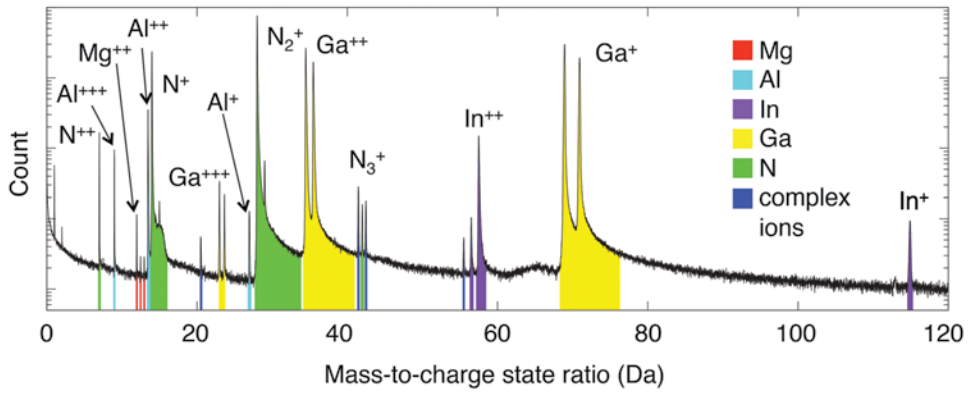


**Figure 4:** Mass spectrum of the GaN LED device obtained by APT. The Ga peaks (yellow) appear in both single and double charge states. Note the distinctive 60:40 natural isotopic abundance ratio between $^{69}$Ga and $^{71}$Ga. The N-related peaks (green) include $N^{++}$, $N^{+}$, and $N_2^{+}$. Peaks characteristic of Mg, Al, and In are highlighted in red, cyan, and indigo, respectively. Other complex ions are highlighted in blue.

This was the first microscopy technique to allow the direct observation of individual atoms [16].

In a modern atom probe no imaging gas is used. Instead, the field at the specimen apex is strong enough that surface atoms themselves are ionized and removed. By maintaining a standing field just below the threshold for field evaporation, a voltage (or thermal) pulse can provide the additional field (or thermally lower the necessary field) to initiate field evaporation, thus providing specimen ions for TOF mass spectrometry. In a manner similar to FIM, the evaporated ions are projected approximately orthogonally from the surface, but instead of using a phosphor screen to collect ions, the coordinates of the impact positions and the travel times are recorded by a position-sensitive TOF detector. This combination of information allows the original surface location and mass-to-charge ratio of each ion to be determined.

## Specimen Preparation

**Sharp tip specimens.** With many microscopy techniques a successful measurement starts with good specimen preparation, and APT is no exception. There are two principal ways that specimens can be created for atom probe analysis. The more traditional method of electrochemical polishing is generally restricted to metal samples [17]. More modern methods use focused ion beam (FIB) lift-out techniques, which allow the creation of atom probe specimens from a wide range of materials and inherently enable site-specific sample preparation [18,19]. The process of turning a commercial device into an APT specimen is truly a process made possible by modern nano-technology.

Because the object of this study was a commercial product purchased from a retail supplier (OSRAM 455 nm Golden Dragon® Plus), the GaN wafer needed to be depackaged from the surrounding superstructure before performing FIB lift-out. As shown in Figure 2a, the LED chip was bonded into a package with wires and encapsulated with a plastic lens. Despite this, reaching the wafer was actually straightforward. Mechanical polishing stripped away the epoxy and exposed the device, as shown in Figure 2b.

**Region of interest.** The next challenge was to locate the region of interest (ROI) within the full GaN device depth. The SEM micrographs of a section of the GaN material, shown in Figures 2c and 3 (left), give some initial indication of the device structure, with image contrast revealing two planar features. The active region of the LED is expected to contain both aluminum and indium alloys, so an SXFiveFE electron probe micro analyzer (EPMA) was used [Figure 3 (center and right)] to look for these elemental signatures. The two layers showing contrast in the SEM image correspond to regions containing aluminum; however, only one of the layers also gave a signal for indium (Figure 3 right).

**Final steps.** Final extraction and placement of the ROI within a sharp specimen tip was performed using routine FIB procedures [20–21]. In this case, the specimen was inverted prior to mounting and sharpening to prevent a layer with poor adhesion from being present in the final specimen tip [22]. The extracted and inverted material was placed on posts on a microtip coupon (Figure 1c), the result of which is shown in Figure 2d. The final specimen shape was formed by annular milling to form a tip (Figure 2e) and then low-energy ion milling until the ROI was within ~100 nm of the surface. Figure 2f shows a fully prepared specimen.

## Data Acquisition

The sample was cooled to 25 K, and field evaporation was achieved with the assistance of a 355 nm laser, pulsing at 500 kHz in a LEAP 4000X Si™. Each pulse had a duration of $10^{-11}$ s with pulse energies adjusted during the course of the measurement

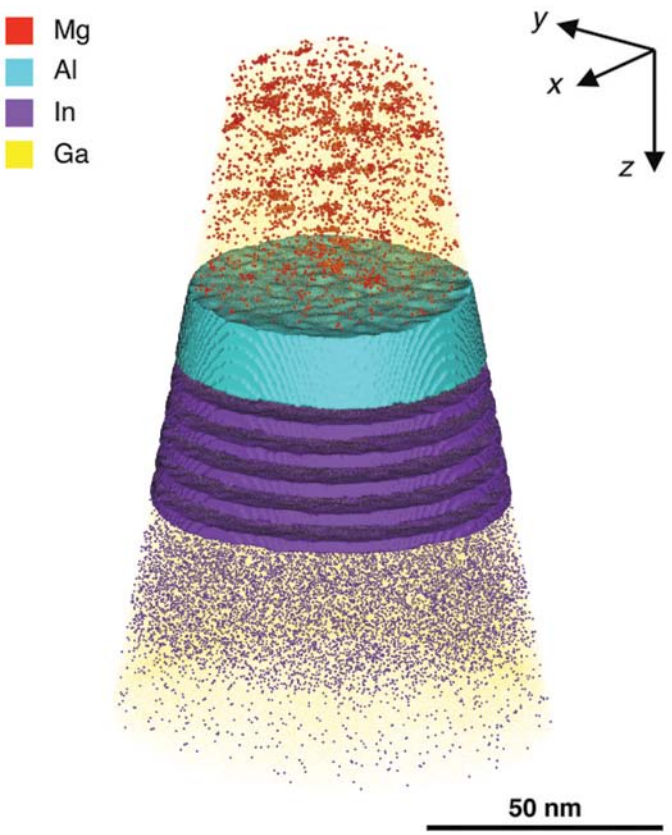


**Figure 5:** Atom cloud of the reconstructed dataset. Single points mark the position of a detected atom. Mg is represented by red, Al by cyan, In by indigo, and Ga by yellow. For clarity only the cations are shown. Isosurfaces indicate volumes containing concentrations greater than 3.0 at.% Al and 3.0 at.% In.

from 3 to $70 \times 10^{-15}$ J to maintain a constant temperature at the apex. Under these conditions, good stoichiometry was found between the two principal matrix elements, Ga and N. A total of 45 million atoms were collected in less than 90 minutes of acquisition time. Reconstruction, visualization, and analysis of the atom probe data were then conducted using the IVAS™ software suite [23].

The mass spectrum of the analyzed volume, Figure 4, shows that the device is composed of a number of elements in addition to Ga and N. As expected from the EPMA compositional profiling, In (0.95 at.%) and Al (0.75 at.%) are present as well as Mg (0.014 at.%). The natural isotopic abundances of In and Mg are reflected in the APT data.

## Results

Besides determining bulk composition, the unique strength of APT lies in its ability to determine compositions in 3D. Figure 5 shows an atom cloud of the reconstructed dataset. A complex structure is apparent. Figures 6a–c show one-dimensional (1D) elemental compositional profiles generated from within the reconstructed volume.

**Four distinct regions.** Four distinct regions are identified, labeled α through δ, each with different alloy concentrations. Volume α contains the Mg required to create the p-doping, forming carriers for injection into the active light-producing region. In fact, producing p-type GaN is a technological challenge, and Mg is almost exclusively used for this task [24]. Volume β contains some Al. We would expect this element to substitute into cation positions in the GaN crystal, and indeed the increase in Al concentration is matched with a corresponding decrease in Ga. An AlGaN alloy is commonly used as an EBL between the active layer and the p-doped region. Volumes γ and δ contain In, in respectively greater and lesser concentrations. The former is identified as an InGaN MQW structure used as the active region.

For an LED device, there must be both a p-type and n-type volumes. The deepest region in Figure 7a, volume δ, contains In, which is neither a donor nor an acceptor, so this cannot be the n-type region. The most common donor dopants for GaN are Si or O, although other elements such as Ge or Sn can be used. Because none of those possible n-type dopants were detected, it is likely that in the case of this particular analysis the volume either does not include the n-type layer or the n-type dopant is obscured in some way. In APT, $^{28}Si$ doping is difficult to quantify within GaN because of the mass-spectral overlap of the $^{28}Si^{++}$ and $^{28}Si^{+}$ ions with the abundant $^{14}N^{+}$ and $^{14}N_2^{+}$ ions.

## Data Analysis

**p-type layer.** Region α accounts for the detected Mg and contains negligible Al or In. Measurements of the bulk composition of this region find that 0.070 at.% of the detected atoms are Mg; that is, a doping density of $6.2 \times 10^{19}$ atoms/cm$^3$. However, by visual inspection, the Mg atoms shown in Figure 7a do not appear to be uniformly distributed. There are various ways of performing cluster identification on APT datasets [25], but for this demonstration regions of high Mg concentration are highlighted by isoconcentration surfaces. In Figure 7b, these isosurfaces show volumes that contain Mg concentrations >1 at.%. A total of 32 such Mg-rich clusters are identified in this volume. Examining the concentration inside the clusters finds that the Mg doping can locally reach as high as 10 at.%.

The formation of clusters will have implications for the electrical properties of the material, affecting the p-type conductivity. Some of the Mg in this structure may be rendered inactive and not act as an acceptor. By counting the Mg atoms inside and outside the clusters separately, it is found that 36% of Mg atoms are concentrated within the clusters. The heterogeneity of the doping is certain to impact device design and performance, so it would be informative to correlate this structure and composition with electrical characterization.

**Electron blocking layer.** Region β contains a high concentration of Al, about 10 at.% of the detected atoms in the volume, creating an EBL. The close-up view of the 1D profile in Figure 6c suggests some additional structure to the layer: the upper interface (β1) has a broad profile, whereas the lower interface (β2) has a narrow layer with a greater Al enrichment, increasing up to 14 at.%, followed by a sharper interface profile. Quantitative measurements of the roughness of the 5 at.% Al isosurfaces shown in Figure 8 finds that the top interface RMS roughness of $R_{RMS}(\beta 1) = 0.71$ nm, whereas for the lower interface $R_{RMS}(\beta 2) = 0.17$ nm. These

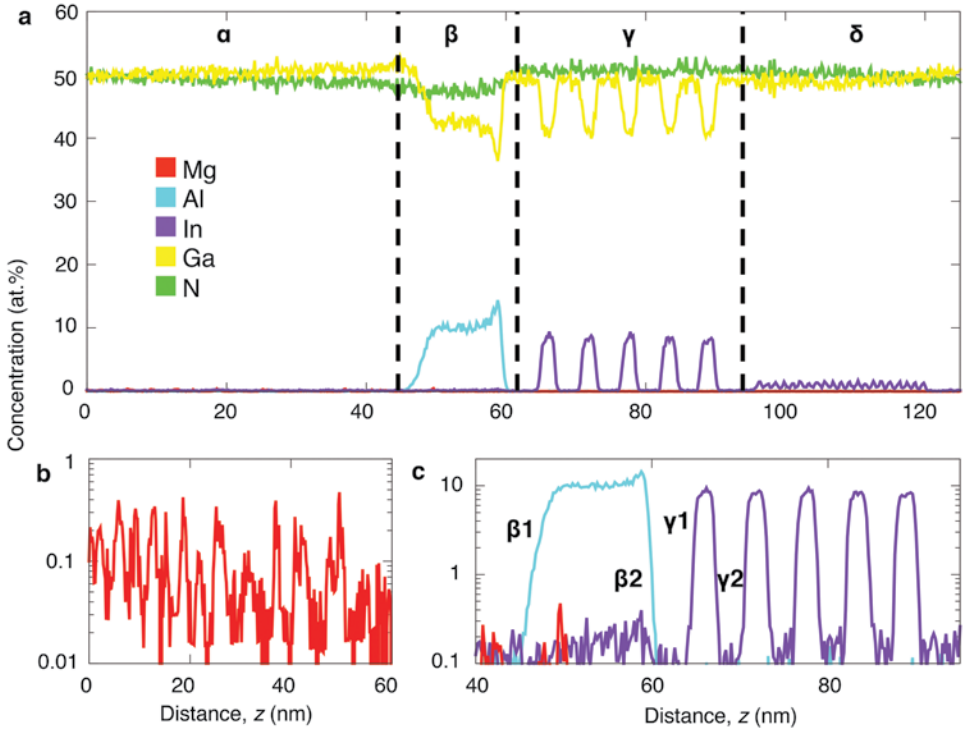


**Figure 6:** (a) One-dimensional composition profiles of the data shown in Figure 5. Four distinct regions are evident from the profile. Region α is composed of 0.07 at.% Mg ions in addition to the GaN matrix; a close-up of this profile is shown in (b). β contains 10 at.% Al ions. γ contains a high concentration (7.2 at.%) of In ions in a periodic structure. A close-up of this region is shown in (c), with the interfaces between the doped and undoped regions respectively labelled. δ contains a low concentration of In atoms.

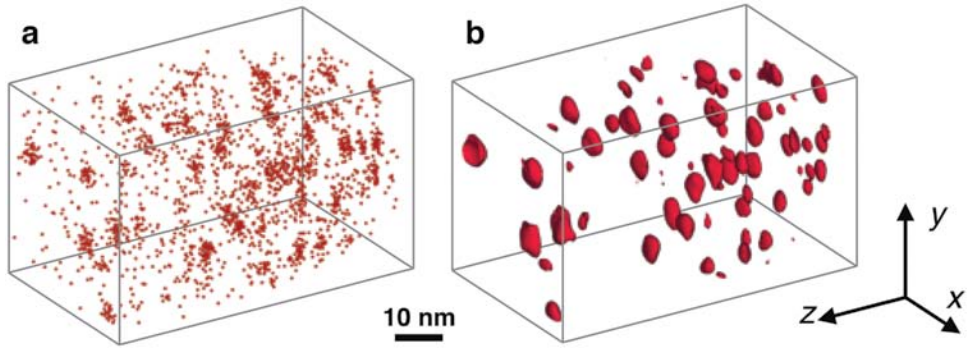


**Figure 7:** A 40×40×67 nm$^3$ sub-volume of region α. (a) atom map displaying only the Mg atoms, rendered as 0.3 nm radius spheres. (b) isosurfaces surrounding volumes containing >1 at.% Mg, indicating the location of Mg clusters.

differences could be unintended defects resulting from the layer growth, as the previously discussed Mg clusters likely are, or perhaps this is evidence of a further efficiency-enhancing mechanism. Without any knowledge of the original design or expected growth results, it is not possible for us to say, but a device engineer might want to investigate the optoelectronic properties to determine whether this structure is desirable for promoting hole injection and preventing electron leakage.

Furthermore, we find that there is some Mg present in region β. As with region α, the Mg is not uniformly distributed but has formed into clusters located near top interface β1. Excluding the clusters, the Mg doping in the EBL is ~0.02 at.%. There also appears to be some Mg, ~0.01 at.%, in a 7 nm layer of GaN between the bottom of the EBL (β2) and the start of the first InGaN QW (γ1). In the rest of the MQW structure, if there is any Mg present, it is at levels below the detection limit of the measurement. Thermal load during processing can potentially result in unwanted diffusion and intermixing, so it is important to correlate dopant distribution to device performance.

**Multiple quantum well.** In volume γ, the InGaN MQW, the average In concentration within the five QWs is determined as 8 at.%. Similar to the analysis of the AlGaN interfaces, Figure 8 also shows an example of a measurement of the roughness of the interfaces of the first layer in the MQW, labeled γ1 and γ2. No significant difference is found between the mean $R_{RMS}$ values of the top and bottom interfaces. Notably, there are also no detected 3D inclusions in the InGaN layers, which would manifest as protrusions in γ1, γ2, or the subsequent layers. Either these patented structures are not being used in this device, or the planar density is low enough that none were present in the field of view of this measurement.

**Superlattice.** The bulk In doping in volume δ is 0.83 at.% (Figure 6a), but a close-up of the atom map shown in Figure 9a indicates a laminar structure. The 1D profile in Figure 9b confirms the In concentration varies periodically between 0.5 at.% and 1.5 at.%. There are 21 In-rich layers with an average spacing of 1.5 nm. This feature is therefore recognized to be an SL, although the authors may only speculate on its intended purpose in this specific device.

## Conclusion

We have used APT to perform a detailed analysis of the atomic composition of a commercial semiconductor device: an OSRAM 455 nm Golden Dragon Plus LED. The APT analysis reveals a varied and complex structure in the light-emitting region of the device, but, more importantly, the data unambiguously determines key details of the device and the efficiency-improving technologies that have been included. Features include Mg doping to form p-type GaN; an Al-rich EBL; an In-rich 5-period MQW; and an In-based SL, with thicknesses on the order of only a few nm. In particular, the clustering of the Mg dopants and the

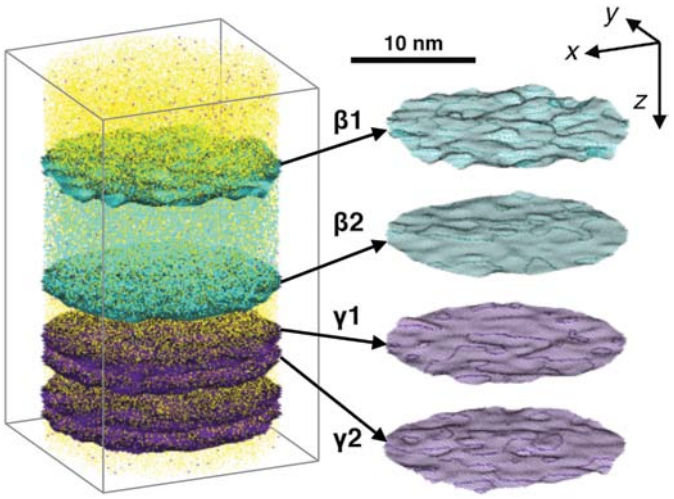


**Figure 8:** A 30×30×50 nm$^3$ sub-volume of regions β and γ. Ga atoms are displayed in yellow, Al in cyan, and In in indigo. Isosurfaces show 5 at.% Al and 4 at.% In concentrations. Wireframes of the interfaces are extracted (shown here β1, β2, γ1, and γ2), and RMS roughnesses are calculated as $R_{RMS}(\beta1) = 0.71$ nm, $R_{RMS}(\beta2) = 0.17$ nm, $R_{RMS}(\gamma1) = 0.28$ nm, and $R_{RMS}(\gamma2) = 0.24$ nm.

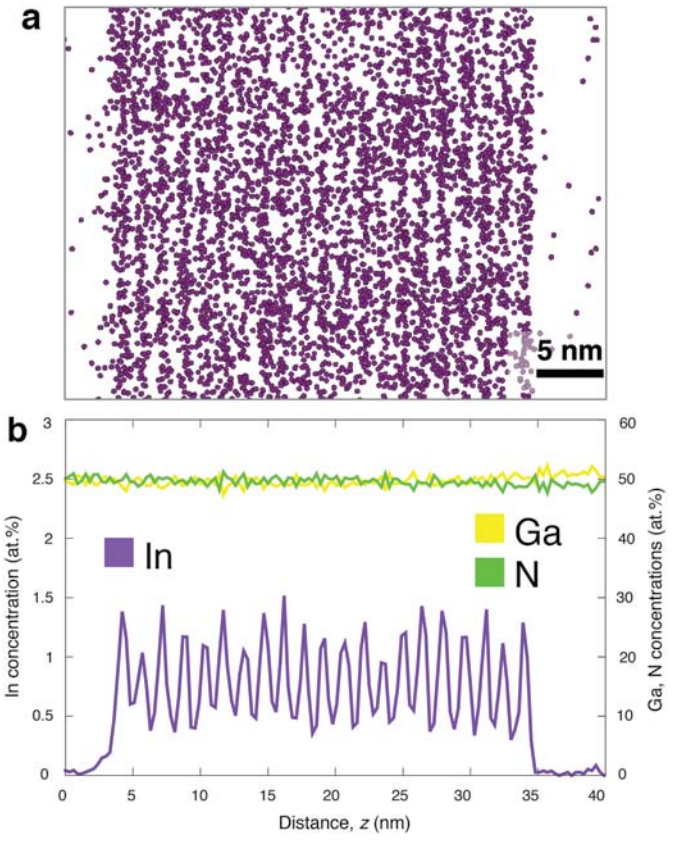


**Figure 9:** (a) A close-up of 40 nm deep volume of region δ, with the atom map showing only the In atoms, which appear to be in a periodic structure. (b) 1D concentration profile shows there are 21 In-rich layers separated by 1.5 nm, with the In concentration varying from ~0.5 at.% to 1.5 at.%.

short-period SL are both structures that would be very difficult to directly detect using other techniques.

Detailed analysis can been conducted on these features to assess the 3D composition, dopant clustering, segregation, interface roughness, and other structural features that would be of interest to an engineer conducting competitive/failure analysis. The relative ease with which such detailed analyses can now be obtained on previously secret devices should have widespread implications in both electronics manufacturing and other industries.

## References


[1] Axis Research Mind, "Global Consumer Electronics Market Trends, Estimates and Forecasts, Report 2011-2018," ARMMR196, Nov. 2013.

[2] U. S. Federal Trade Commission. *To Promote Innovation: The Proper Balance of Competition and Patent Law and Policy,* DIANE Publishing, Darby, PA, 2003.

[3] Nichia Corporation, "Nichia Asserts Design Patents Against Seoul Semiconductor," Jan. 16, 2006, http://www.nichia.co.jp/en/about_nichia/2006/2006_011601.html (accessed February 24, 2014).

[4] Nichia Corporation and Seoul Semiconductor, "Nichia And Seoul Semiconductor Settle Litigation And Enter Into a Cross-License," Feb. 2, 2009, http://www.nichia.co.jp/en/about_nichia/2009/2009_020201.html (accessed Feb. 24, 2014).

[5] TF Kelly and DJ Larson, *Annu Rev Mater Res* 42 (2012) 1–31.

[6] DJ Larson et al., *Journal of Physics: Conference Series* 471 (2013) 012030.

[7] J Wu et al., *Appl Phys Lett* 80 (2002) 3967–69.

[8] W Walukiewicz et al., "Structure and electronic properties of InN and In-rich group III-nitride alloys" *J Phys Appl Phys* 39 (2006) R83.

[9] Z Chen et al., Laterally contacted blue LED with superlattice current spreading layer. US Patent 8395165 B2, filed July 8, 2011, published Mar. 12, 2013.

[10] Z Chen, LED having a low defect n-type layer that has grown on a silicon substrate. WO Patent 2013019318 A1, filed June 9, 2012, published Feb. 7, 2013.

[11] CH Lee et al., Light emitting diode having a barrier layer with a superlattice structure. US Patent 8575594 B2, filed Feb. 27, 2012, published Nov. 5, 2013.

[12] T Udagawa, Semiconductor light-emitting diode. US Patent 8299451 B2, filed Nov. 2, 2006, published Oct. 30, 2012.

[13] JM Gerard and C Weisbuch, Semiconductor structure for optoelectronic components with inclusions. US Patent 5075742 A, filed Jan. 10, 1991, published Dec. 4, 1991.

[14] *Seoul Semiconductor Co. LTD. v. Nichia Corp*., 590 F. Supp. 2d 832 (E.D. Tex. 2009).

[15] EW Müller et al., *Rev Sci Instrum* 39 (1968) 83–86.

[16] EW Müller, *J Appl Phys* 27 (1956) 474–76.

[17] EW Müller and TT Tsong, *Field ion microscopy: principles and applications*. American Elsevier Pub. Co., New York, 1969.

[18] HO Colijn et al., *Microsc Microanal* 10 (2004) 1150–51.

[19] MK Miller et al., *Ultramicroscopy* 102 (2005) 287–98.

[20] K Thompson et al., *Microsc Microanal* 12 (2006) 1736CD.

[21] K Thompson et al., *Ultramicroscopy* 107 (2007) 131–39.

[22] TJ Prosa et al., *Microsc Microanal* 15 (2009) 298–99.

[23] DJ Larson et al., *Local Electrode Atom Probe Tomography: A User's Guide*. Springer, New York, 2013.

[24] H Amano et al., *Jpn J Appl Phys* 28 (1989) L2112–14.

[25] B Gault et al., *Atom Probe Microscopy*, Springer, New York, 2012.

# Right results...Real-time



**Only Oxford Instruments has the expertise to deliver:**

- Large area detectors that deliver outstanding speed and sensitivity
- Algorithms that automatically and accurately identify all the elements
- Process engines that deliver the correct results in real-time...every time

*Right results in real-time ...it's what we do!*

**To see how to obtain the right result visit www.oxford-instruments.com/results**

OXFORD INSTRUMENTS

*The Business of Science®*

https://doi.org/10.1017/S1551929514000819 Published online by Cambridge University Press